Thermoconvectional phenomena induced by vibrations in supercritical SF_6 under weightlessness

Y. Garrabos,[1] D. Beysens,[2,3] C. Lecoutre,[1] A. Dejoan,[1] V. Polezhaev,[4] and V. Emelianov[4]
[1]*ESEME, Institut de Chimie de la Matière Condensée de Bordeaux, UPR 9048 CNRS, Université Bordeaux I, 87, Avenue du Dr. Schweitzer, F-33608 Pessac Cedex, France*
[2]*ESEME, Service des Basses Températures, Direction des Sciences de la Matière, CEA-Grenoble, F-38054 Grenoble Cedex 9, France*
[3]*ESEME, ESPCI-PMMH, 10, rue Vauquelin, 75231 Paris Cedex 5, France*
[4]*Institute for Problems in Mechanics, Russian Academy of Sciences, Prospect Vernadskogo 101, 117526, Moscow, Russia*
(Received 19 June 2006; revised manuscript received 10 November 2006; published 31 May 2007)

The effect of a linear harmonic vibration on heat propagation is investigated in near-critical SF_6 under weightlessness conditions in space. Heat was issued from a pointlike source (thermistor), a situation representative of an industrial use of pressurized supercritical fluid storage. Two kinds of vibrations were used, large amplitude (64 mm) at 0.2 Hz and low amplitude (0.8 mm) at 1.6 Hz, with temperatures from 5 K to 20 mK from the critical temperature. The vibrations are seen to strongly affect the evolution and shape of the hot boundary layer (HBL), the heat exchange between the heat source and the fluid, and the bulk thermalization process by the adiabatic piston-effect process. The HBL is initially convected as symmetrical plumes over a distance that only depends on the vibration velocity and which corresponds to a Rayleigh-Bénard-like instability where the vibration acceleration acts as the earth gravity. Then the extremities of the plumes are convected perpendicularly to the direction of oscillation as two "pancakes," a process encountered in the vibrational Rayleigh-Bénard instability. When the vibration velocity is small, only one pancake centered at the hot source is observed. Temperature evolutions of the hot source and the fluid are studied in different locations. Convection flows and adiabatic piston effect compete to determine the thermal dynamics, with the latter being the most efficient near the critical point. The experimental results are compared with a two-dimensional numerical simulation that highlights the similarities and differences between the very compressible van der Waals gas and an ideal gas.

DOI: 10.1103/PhysRevE.75.056317 PACS number(s): 47.20.Bp, 47.15.Rq, 47.32.C−, 05.70.Jk

I. INTRODUCTION

Vibrations are very often used in industry as an empirical way for controlling solid-solid, liquid-solid or liquid-liquid dispersions. The role of gravity is always important. In contrast, the thermal processes activated by vibrations in fluids when gravity effects are absent have been only poorly studied, and almost essentially from a theoretical point of view [1]. Such vibrations, however, can generate average flows that show some similarities with earth gravity driven convections. In this sense, vibrations might appear as a way to control and operate fluids in space by creating effects similar to those triggered by earth gravity.

It is the subject of this paper to investigate basic thermal processes in a fluid under weightlessness submitted to the harmonic linear vibration

$$X = B\ \sin(\omega t). \tag{1}$$

Here X is the spatial coordinate, B is the amplitude, $\omega = 2\pi f$ is the angular frequency with f the frequency and t the time.

We consider a fluid in the vicinity of its critical point. Such vicinity is indeed particularly interesting. There is currently a strong interest from the space industry to use fluids in orbit in their supercritical conditions where they can be operated in one liquid densitylike single phase. In addition, such fluids exhibit a number of unusual thermodynamics and transport phenomena when they are set in near-critical conditions. They then behave quite differently from ideal gases. For example, on the critical isochore, the thermal conductivity λ and the specific heats at constant pressure C_p and constant volume C_V diverge, whereas the thermal diffusivity D_T tends to zero. The fact that the fluid becomes also very compressible and expandable emphasizes the process of adiabatic heating or "piston effect" [2]. This process takes place during heating (or cooling) when the diffusive thermal boundary layer expands (or contracts) and pressurizes (or depressurizes) the outer bulk fluid, resulting in a very fast adiabatic thermalization. The associated "critical speeding up" of the fluid thermalization that occurs at constant volume, contrasts with the classical thermal "critical slowing down," a phenomenon at constant pressure.

Preliminary experiments [3] under weightlessness with near critical fluids have shown that vibrations were able to induce a rich set of phenomena. In the present study, we focus on the development of a hot boundary layer (HBL) in heated SF_6, under harmonic vibration of (i) large amplitude, low frequency and (ii) small amplitude, high frequency.

II. EXPERIMENT

A. Experimental setup

The experiments were carried out with the automatic ALICE-2 facility onboard the Mir station (Fig. 1). The ALICE-2 instrument provides optical (e.g., interferometer) and thermal diagnoses, including thermal control within a few μK in the temperature range $T = 293 - 343$ K. For more details, see [4]. The experimental cell used for this study was made of a $CuCo_2Be$ alloy. The internal fluid volume is a

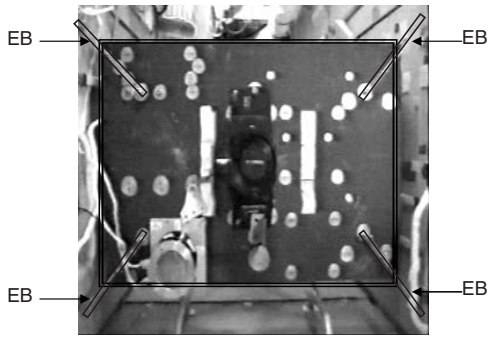

FIG. 1. The facility ALICE-2 is attached to the walls of the "Priroda" module of the Mir station by elastic belts (schematized by EB) and excited at the resonance frequency.

cylinder ($2R=12$ mm internal diameter, $e=6.79$ mm thickness) sandwiched between two parallel sapphire windows (12 mm external diameter), the inner surface of one of which being covered with a dielectric coating to create a mirror. The cell is filled at critical density ρ_c within 1% and its critical temperature is measured before flight within 1 mK. Several previous experiments have shown that the T_c drift with time was negligibly small in such samples. We thus imposed with confidence the value before flight in all our programmed experiments. In-flight visual observations were indeed in agreement with the above value.

Three thermistors (Thermometrics B10, 10 ms risetime, 500 μK accuracy, $2r_0=d_0=0.2$ mm diameter) are set in the cell to measure local fluid temperatures (Figs. 2–5). Two of them (labeled Th1 and Th2, local temperature T_1 and T_2, respectively) are mounted at the end of a hair-pin thread and located at a close distance from the cell wall (Th1, 1 mm, Th2, 1.5 mm). The third thermistor (Th3, local temperature T_3) is mounted in the middle of a rectilinear thread which is placed on a diameter at half-thickness of the cell. It is also used as a central heat source, in an arrangement commonly encountered in gas tanks. Temperature in Th3 cannot be measured during heating. The frequency of the temperature measurements is 25 Hz during the first 5 minutes following heating, then 0.1 Hz during the next 55 minutes. The image of the sample is obtained through a Twyman-Green interferometer and is recorded by a CCD camera at a frequency of 25 Hz.

In order to impose a sinusoidal oscillation to the fluid, the ALICE-2 instrument (mass around 60 kg) was suspended with rubber belts inside the "Priroda" module in the Mir orbital station (Fig. 1). A periodic resonant movement is excited close to the center of mass of the instrument, either manually or by an electronically controlled shaker (mass around 4 kg). Varying the tension and the number of the belts change the resonance frequency. One end of each belt is tightened to a corner of the ALICE-2 instrument, the other end is secured to a wall of the compartment. A three-axes

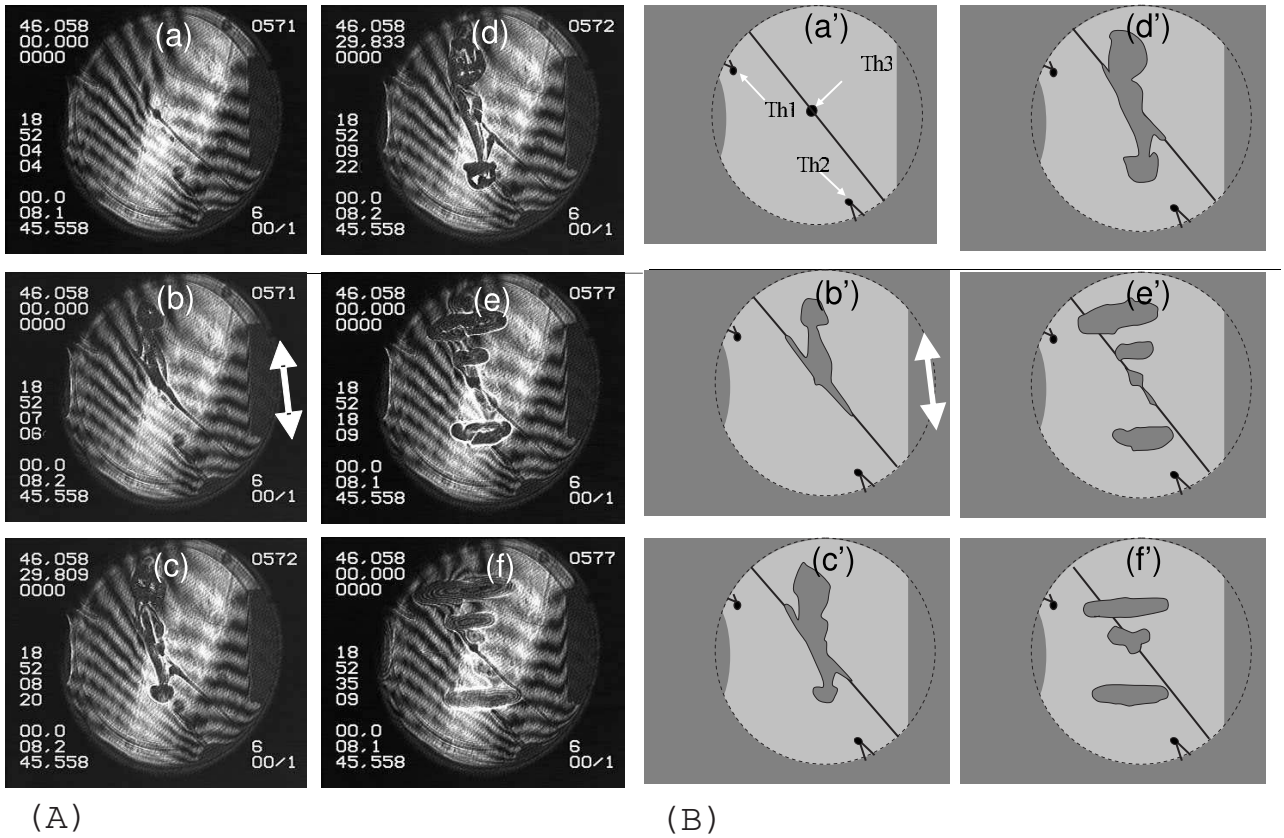

FIG. 2. Spreading of the HBL at $T-T_c=500$ mK during a vibration V′1 (3.6 s heat pulse, 0.828 mW power). (A) Observations: (a) $t=0$, (b) $t=3.08$ s after starting the heat pulse. The double arrow indicates the direction of vibration: (c) $t=4.64$ s, (d) $t=5.72$, (e) $t=14.2$ s, (f) $t=31.2$ s. (B) Schematic: Here $(a')-(f')$ indicate the same sequence as in part (A). The arrows in (a') indicate the location of the three thermistors. The large double arrow in picture (b') again indicates the direction of vibration.

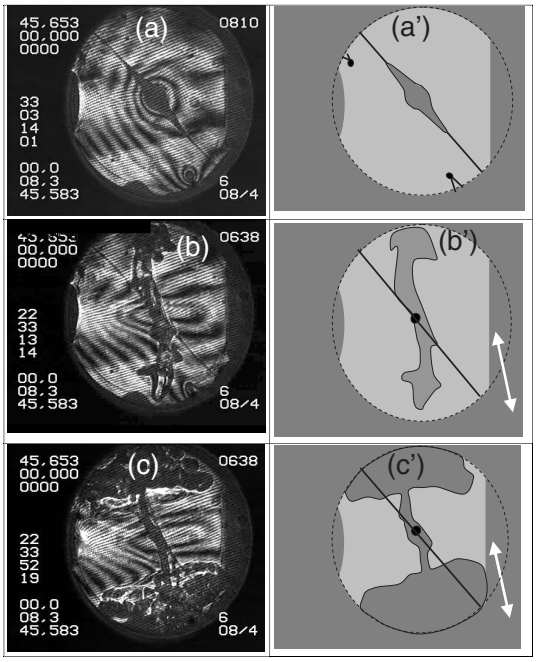

FIG. 3. Spreading of the HBL during the heating of the thermistor (120 s time duration, 0.828 mW power). (a) Without vibration, $T-T_c=0.1$ K, $t=10$ s after the start of the pulse, (b) under vibration V1, $T-T_c=0.1$ K, $t=9.4$ s after the start of the heat pulse. The double arrow indicates the direction of vibration. The HBL is convected as a double plume. (c) $t=48.6$ s after the start of the heat pulse. $(a')-(c')$ *id*, schematic.

microaccelerometer measures the acceleration levels at 25 Hz in the range $0.1-10^{-6}g$ ($g=9.81$ m s^{-2} is the earth acceleration value). Manual excitation (labeled V1) yields a frequency $f=0.2$ s^{-1} and an amplitude $B=64$ mm (acceleration amplitude $10^{-2}g=0.10$ m s^{-2}, velocity amplitude $B\omega=80$ mm s^{-1}). The shaker excitation (labeled V2) provides $f=1.6$ s^{-1} and $B=0.8$ mm (acceleration amplitude

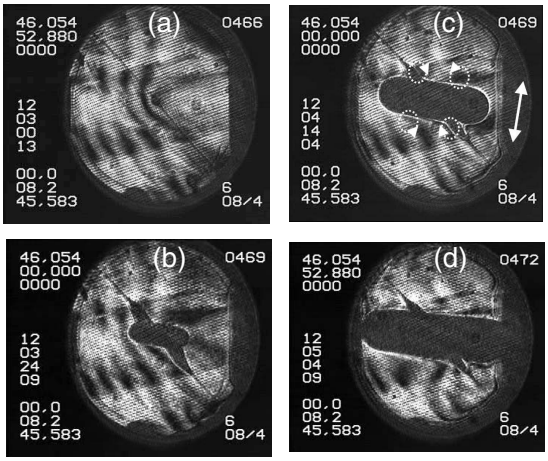

FIG. 4. Spreading of the HBL at $T-T_c=0.5$ K during a vibration V2 (120 s heat pulse, 0.828 mW power). (a) Before starting the heat pulse. (b) $t=20$ s and (c) $t=70$ s. The double arrow indicates the direction of vibration. The circles that are drawn correspond very schematically to the presence of four counter-rotative convection rolls (see the discussion in the text and Fig. 11). (d) $t=120$ s.

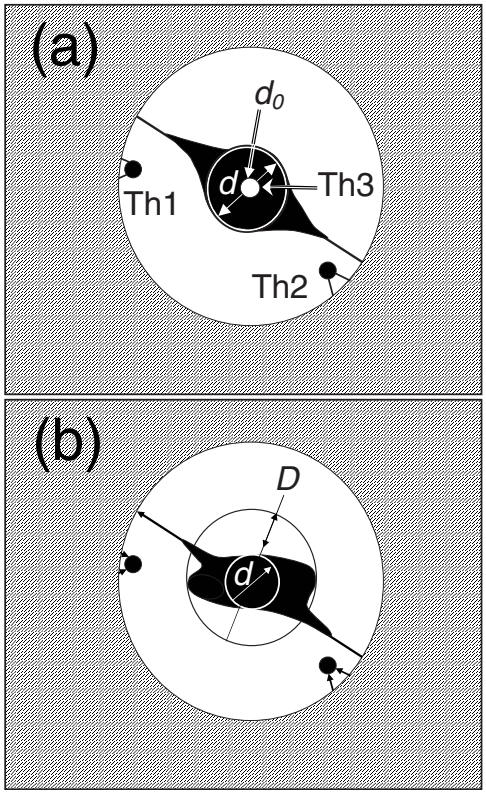

FIG. 5. Schematic representation of the hot boundary layer inside the cell. (a) Without vibration NV [see also Fig. 3(a)] and (b) in the presence of vibration V2 (see Fig. 4). Th1,2,3 are thermistors. Th3 is also used as a heat source.

$8.24\times10^{-3}g=0.0808$ m s^{-2}, velocity amplitude $B\omega=8.04$ mm s^{-1}), see Table I.

B. Experimental procedure

The experiments have been carried out at 5 reduced temperatures $T-T_c=5$ K, 500 mK, 100 mK, 50 mK, 20 mK (see Table II), according to the vibration and heat pulse conditions as reported in Table I. During each run of about 30 hours, heat pulses of $P_0=0.828$ mW electric power and $\delta t=120$ s duration were performed. After each pulse, the sample was left for a time sufficient for equilibration, 1 hour at T_c+5 K, 5 hours at T_c+20 mK. Density equilibration can be checked in the interferometer image. The heat pulses with no vibration (labeled NV) were performed under calm conditions (acceleration $\leqslant10^{-4}g$), when the cosmonauts were

TABLE I. Summary of the experiments reported here. V1, V′1, and V2 label the vibration conditions (see text). Label NV means the absence of vibrations.

Excitation	B (mm)	f (s^{-1})	δt (s)	P_0 (mW)
V1	64	0.2	120	0.828
V′1	64	0.2	3.6	0.828
V2	0.8	1.6	120	0.828
NV	0	0	120	0.828

TABLE II. Summary of the experimental conditions and critical power law behavior for useful thermophysical properties of SF_6 (from [5]). $\tau=(T-T_c)/T_c$ is the reduced temperature difference. For the notations, see text. V1, V′1, V2, and NV label the vibration conditions (see Table I).

Excitation type	V1 NV	V′1 V2 NV	V1 V′1 NV	V′1 V2 NV	V2 NV
$T-T_c$ (mK)	5000	500	100	50	20
t_D (s)	900	4200	12400	19800	36500
t_{PE} (ms)	20900	414	31	10	2.4
t_ν (s)	47	43	40	39	38
$t_{\eta b}$ (ms)	0.12	0.6	2.0	3.3	6.4
T_c (K)			318.735		
ρ_c (kg m^{-3})			740.2		
ξ (m)			$1.93\times10^{-10}\tau^{-0.63}$		
β_P (K^{-1})			$1.01\times10^{-3}\tau^{-1.24}$		
K_T (Pa^{-1})			$1.22\times10^{-8}\tau^{-1.24}$		
$(\partial P/\partial T)_\rho$ (Pa K^{-1})			8.35×10^4		
C_V (J Kg^{-1} K^{-1})			$491.66\tau^{-0.11}$		
c (m s^{-1})			$90.82\tau^{-0.055}$		
$\gamma_0=C_p/C_V$			$0.070\tau^{-1.13}$		
D_T (m^2 s^{-1})			$4.02\times10^{-8}\tau^{0.67}$		
ν (m^2 s^{-1})			$4.05\times10^{-8}\tau^{-0.04}$		
η_b (Pa s)			$1.97\times10^{-7}\tau^{-1.82}$		
L (mm)			1.5 [see Eq. (4)]		

asleep. We will not discuss here other sequences of pulses with lower injected power and/or shorter duration. These data all support the following analysis although they exhibit larger uncertainties in the temperature measurements. We will, however, consider one case identical to V1, but with a heat pulse of much shorter time duration $\delta t=3.6$ s, hereafter labeled V′1 (see Table I).

III. RESULTS AND DISCUSSION

In the following we analyze the spatial extension of the hot boundary layer for the excitation modes V1, V′1, V2, and NV, and the evolution of the T_1, T_2, and T_3 temperatures.

A. General about thermalization

In fluids under weightlessness maintained at constant volume, heat transfer may be performed by both thermal diffusion and adiabatic compression. This mechanism was called the "piston effect" (PE) because the diffusing HBL acts as a piston to heat the interior of the fluid [6,7]. The HBL is a region of density gradient that manifests itself in the interferometer pictures as a black area around the heat source Th3, with a sharp interface [Figs. 3(a) and 3(a′)]. In the absence of vibration, the HBL is nearly spherical in shape if we exclude the heated regions along the lead wires. It spreads diffusively [8].

As the critical point is neared, the heat diffusion slows down whereas the PE speeds up the thermalization. The latter process is then dominant in near-critical fluids, leading to a very fast thermalization. The adiabatic nature of the fast thermal equilibration in supercritical homogeneous fluid samples has been confirmed by numerous experiments [8–15], many of them performed in weightlessness where convection is absent, and is now well established.

Let us define t_D, the typical diffusion time on length scale L [defined below in Eq. (4)] as

$$t_D=\frac{L^2}{D_T}\sim\tau^{0.67}, \tag{2}$$

where D_T is the thermal diffusivity that tends to zero as the reduced temperature $\tau=(T-T_c)/T_c$ goes to zero (Table II).

Thermalization by the PE occurs after the characteristic time t_{PE} such as

$$t_{PE}=\frac{t_D}{(\gamma_0-1)^2}\sim\tau^{1.59}. \tag{3}$$

Here $\gamma_0=C_p/C_V\sim\tau^{-1.13}$ diverges as τ tends to zero (Table II). A striking result is thus the critical speeding up of the PE when going closer to the critical point. As a matter of fact, near T_c, γ_0 diverges and t_{PE} goes to zero although t_D goes to infinity. This result represents an enormous gain in the time required by the bulk fluid to come close to the temperature equilibrium. The fluid inhomogeneities (HBL), however, still

relax diffusively [8,13–15], which makes the ultimate density equilibration determined by the diffusion time scale t_D.

The typical length L in the PE is the typical length scale of the HBL near thermalization and can be approximated, according to [15], by the ratio of the sample volume V to the sample external surface S, such as, in the present experimental situation,

$$L \approx \tfrac{1}{2}(e^{-1} + R^{-1})^{-1}. \tag{4}$$

Another PE viscous time $t_{\eta b}$, describing the time delay that the viscous stress imposes to the free expansion of the thermal layer, can also matter. According to [16], this time can be written as

$$t_{\eta b} = [t_{\mathrm{PE}}(4\eta/3 + \eta_b)K_T]^{1/2} \sim \tau^{-0.735}. \tag{5}$$

Here $\eta = \nu\rho$ is the shear viscosity that diverges with a very weak exponent (0.04) near T_c (see Table II). Close to T_c the temperature dependence in Eq. (5) is conditioned by the strong divergence of the bulk viscosity η_b [17–19],

$$\eta_b \approx 0.034\rho c^2 D_T \xi^{-2} \sim \tau^{-1.82}. \tag{6}$$

Here $\xi \sim \tau^{-0.63}$ is the correlation length of density fluctuations (see Table II) and c is the sound velocity, which can be written as

$$c^2 = (1/\rho\kappa_T) + (T/\rho^2 C_V)(\partial P/\partial T)_\rho. \tag{7}$$

The divergence of κ_T makes the first term of Eq. (7) negligible. Taking into account the divergence of $C_V \sim \tau^{-0.11}$ (see Table II) one gets

$$c^2 \sim \tau^{0.11}. \tag{8}$$

The $t_{\eta b}$ values are calculated in Table II for the studied temperature range. Because of the smallness of the prefactor, $t_{\eta b}$ is negligible except very near the critical point (CP), where at 20 mK it is on the order of t_{PE} (see Table II).

However, one must note that the importance of the divergence of the bulk diffusivity is still under debate. There is up to now no direct experimental evidence of this divergence. As noted in Ref. [20], the model can overestimate the role of the bulk viscosity on the thermal boundary layer dissipation. For this reason and the fact that in the studied range the PE viscous time is at most comparable to t_{PE}, we will not consider this PE viscous time anymore.

Another time of interest is the typical viscous time t_ν corresponding to the viscous relaxation of the flow,

$$t_\nu = \frac{L^2}{\nu} \sim \tau^{-0.04}. \tag{9}$$

The parameter ν is the kinematic viscosity that diverges with a very small exponent near T_c; t_ν can thus be considered as nearly constant ≈ 40 s (see Table II).

B. Pattern for V1 and V′1

1. Early times

For vibration regimes V1 and V′1, the HBL is convected at each oscillation along the vibration direction and spreads as two symmetric plumes (Figs. 2 and 3). During the first complete half-period (1.25–3.75 s), a hot plume develops by buoyancy from the hot thermistor with a direction parallel to the vibration direction [vibration V′1, Fig. 2(b)]. During the second complete half-period (3.75–6.25 s), the head of the plume does not return to its initial position. Indeed, the head cannot move back by buoyancy in a plume region that exhibits nearly the same density. At the same time, a symmetric plume rises from the hot thermistor [Fig. 2(c)] and develops as the former plume. The plume stops between the thermistor and the wall, at about 2.4 mm from the thermistor. Figure 3 shows the same phenomenon under V1. The HBL evolution is similar, however, it is noticeable that in this case the plume reaches the cell wall. This phenomenon is then the symmetrical case of what is currently observed on earth (such a convection plume under $1g$ is studied in [21]).

This difference in HBL propagation can be understood as follows. Depending on the buoyancy velocity, which itself depends on the density difference $\Delta\rho$, the plumes are convected on a distance l_p whose value determines whether the plume reaches the cell walls (Fig. 3, V1-type) or not (Fig. 2, V′1-type). Assuming the Stokes velocity V_S for the buoyancy of a hot fluid volume of radius r_0 (the thermistor radius) submitted to the acceleration $B\omega^2$,

$$V_S = \frac{2r_0^2 \Delta\rho B\omega^2}{9\rho_c \nu}, \tag{10}$$

one gets

$$l_p = \frac{V_S}{2f} = \frac{2\pi B\omega \Delta\rho r_0^2}{9\rho_c \nu}. \tag{11}$$

This distance depends only on the vibration velocity $B\omega$. The temperature change at Th3 can be estimated of order on 0.1 K, corresponding to a density inhomogeneity about $\Delta\rho/\rho_c \sim 25\%$ (see below Fig. 7, early times, V1, $T - T_c = 0.5$ K). Inverting Eq. (11) with $l_p = 2.4$ mm (V′1 case) gives indeed $\Delta\rho/\rho_c = 23\%$. The density difference for V1 at 0.1 K from T_c, corresponding to $l_p \sim 6$ mm, would be larger than 60%, which is unphysical. The latter estimation of $\Delta\rho/\rho_c$ simply means that a linear analysis cannot hold for such high temperature rise so close to T_c.

2. Late times

Since the hot fluid cannot be convected in the vibration direction on a distance larger than l_p, it can only spread (i) by diffusion, but it is an extremely slow process, see Table II, and (ii) by convection thanks to the vortices resulting from the viscous coupling with the bulk fluid. The latter process makes the hot fluid spread perpendicularly to the vibration direction at the extremity of the plumes [Figs. 2(d)–2(f) and 3(c)] where hot "pancakes" clearly develop. This case is also reminiscent of what is observed on earth when the interface between hot and cold fluid regions orders in plane layers perpendicular to gravity.

The convective flow that extends the HBL perpendicular to the vibration can also be understood as a vibrational thermal instability of Rayleigh-Bénard-like type [1] in a cell of size R submitted to the temperature difference ΔT. A vibra-

tional Rayleigh number (Rv) can be defined for high frequency vibrations, i.e., vibration period $1/f$ smaller than the typical hydrodynamics times t_D and t_ν, which is precisely the case here, see Table II where $1/f=5$ s, $t_\nu \approx 40$ s, $t_D > 900$ s,

$$\mathrm{Rv} = \frac{(B\omega\beta_P \Delta T R)^2}{2\nu D_T}. \tag{12}$$

A physical meaning of this vibrational Rayleigh number can be found by following the same reasoning that leads to the definition of the classical Rayleigh number. Under earth gravity, a fluid element of size r_0 (the thermistor radius) starts to rise when the typical convective time across the fluid element is shorter than the diffusion time to the surface, that is $\frac{r_0}{V_{sg}} < \frac{r_0^2}{D_T}$. Here V_{sg} is the convective velocity as given by Eq. (10) where the acceleration $B\omega^2$ is replaced by g. The Rayleigh number gives a measure of the ratio of these two diffusive and convective times, $\mathrm{Ra}=g\frac{\beta_P \Delta T L_0^3}{\nu D_T}$. Here one has used the relation $\Delta\rho=\beta_P \Delta T$. Convection starts for $\mathrm{Ra} > 1700$. Let us now consider the same configuration without gravity but under vibration. The criterion for buoyancy-driven convection can be replaced by the presence of a Bernoulli-like pressure difference coming from the velocity difference ΔV between the fluid element and its surrounding, $\Delta P \sim \rho \Delta V^2 = \rho(\Delta\rho/\rho_c)^2 B^2\omega^2$. It results in a driving force $r_0^2 \Delta P$, oriented perpendicularly to the vibration direction. Applying the same procedure used to define the Rayleigh number, another number is obtained, the vibrational Rayleigh number of Eq. (12).

Convection starts for Rv above a critical number Rv_c. According to the reasoning developed above where the Bernouilli pressure drives the convection perpendicular to the vibration direction, the onset of instability will crucially depend on the angle α between the vibration and the temperature gradient direction. When $\alpha=0$, the pressure difference drives any inhomogeneity along the temperature gradient; the inhomogeneity stays at the same temperature. The fluid is thus stable, $\mathrm{Rv}_c=\infty$. (For small α, the asymptotic form is $\mathrm{Rv} \sim \alpha^{-4}$ [1].) When α increases to $\pi/2$, Rv_c decreases to a value of order on 2000, a value comparable to the classical critical Rayleigh number.

For an initially spherical HBL, where the thermal gradient is radial, convection is then the most unstable in the direction perpendicular to the vibration direction. Because of mass conservation, convection rolls eventually form [such rolls have been observed in the simulations on two-dimensional (2D) incompressible and inviscid fluids, see [1] and below].

From the $T-T_c$ dependence of β_P, ν, and D_T (with $R=6$ mm), one gets

$$\mathrm{Rv}_{\mathrm{V1}} \approx 1.3 \times 10^6 (T-T_c)^{-1.77} (\Delta T)^2, \tag{13}$$

where subscript V1 is for vibration V1. In the present experiment, the ΔT value corresponding to the threshold should be on order of 160 mK at $T-T_c=5$ K and 20 mK at $T-T_c=0.5$ K.

Note that the influence of the PE induces a modification related to the Schwarzschild criterion (PE-induced adiabatic temperature gradient) [22]. This adjustment is all the more pronounced as $T-T_c$ is small. How it couples with vibration is beyond the scope of the present study.

C. Pattern for V2

A similar behavior as for vibrations V1 and V′1 is observed for the vibration V2 with much smaller value of the B amplitude. The extension l_p of the plume that is convected parallel to the vibration direction, proportional to $B\omega$, is now reduced by a factor as large as 10. Only the spreading perpendicular to the vibration can thus be observed (Fig. 4). One can estimate the vibrational Rayleigh number to be

$$\mathrm{Rv}_{\mathrm{V2}} \approx 1.3 \times 10^4 (T-T_c)^{-1.77} (\Delta T)^2, \tag{14}$$

where subscript V2 corresponds to the vibration V2.

At 0.5 K from T_c, the temperature gradient at the threshold corresponds to $\Delta T=210$ mK. At 20 mK from T_c, it becomes as weak as $\Delta T=12$ mK (see Fig. 7).

The dynamics of propagation of the HBL can be characterized by its shape evolution. Two typical lengths are $\delta_\perp$ and $\delta_\parallel$, perpendicular and parallel to the vibration direction, respectively,

$$\delta_\parallel = (d-d_0)/2, \tag{15}$$

$$\delta_\perp = (D-d_0)/2. \tag{16}$$

Here d and D are defined in Fig. 5 and d_0 is the thermistor diameter. The evolutions of $\delta_\parallel$ and $\delta_\perp$ are presented in Fig. 6(a) ($T-T_c=500$ mK) and in Fig. 6(b) ($T-T_c=20$ mK). We note the following:

(i) In the absence of vibration (NV), the HBL propagates symmetrically, $\delta_\parallel=\delta_\perp$. These lengths obey a diffusion power law whose exponent is not 1/2 but depends on the temperature range and reflects the nonlinear behavior of the thermophysical properties of the fluid near its critical point [8,23]. The exponents here are 0.42 ± 0.01 ($T-T_c=500$ mK) and 0.48 ± 0.08 ($T-T_c=20$ mK). During this period, the uniform thermalization of the bulk fluid is ensured by the PE.

(ii) Under vibration V2, after a small initial delay, $\delta_\parallel$ increases as can be seen from Fig. 6. The length $\delta_\perp$ increases faster than without vibrations. The slope in the log-log plot of Fig. 6 is of order unity during most of the time where vibration is on. This corresponds to a constant spreading velocity and is indeed the hallmark of a convective flow in the viscous (Stokes law) limit.

D. Heat source temperature relaxation

Temperature measurements at Th3 location are available only when the heat pulse has stopped. We will thus limit the discussion to the relaxation after the heat pulse, when the HBL behavior crosses over from a convective to a diffusive spreading.

Figure 7 shows the typical temperature evolutions of thermistor Th3 [$\Delta T_3(t)=T_3(t)-T_3(\infty)$], without vibration (NV) and for vibrations V1 and V2. One can see in Fig. 7 that T_3 exhibits different behavior depending on the excitation. This

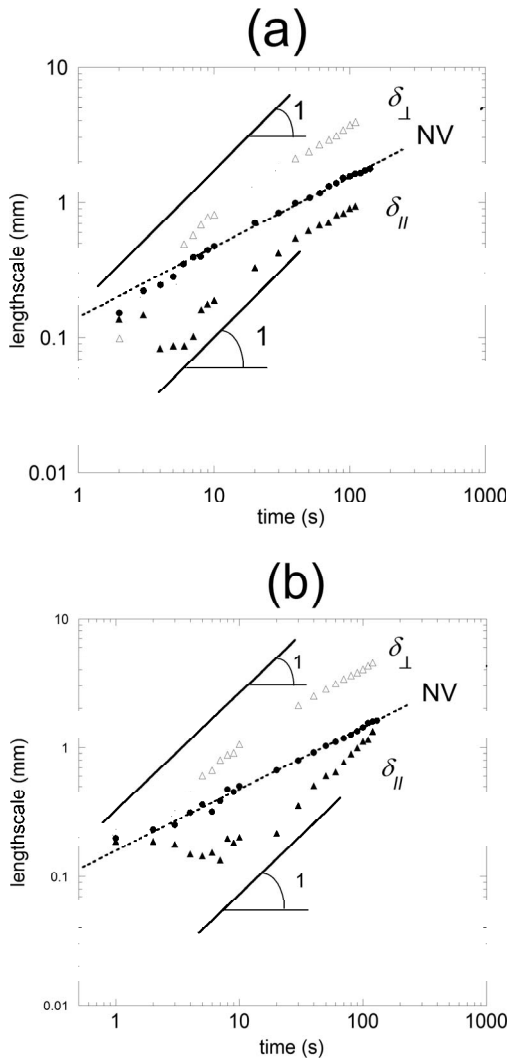

FIG. 6. Evolution (log-log scales) of the HBL length scales $\delta_\perp$ (open triangles) and $\delta_\parallel$ (black triangles) for excitation V2 and NV (black dots). (a) $T-T_c=500$ mK and (b) $T-T_c=20$ mK.

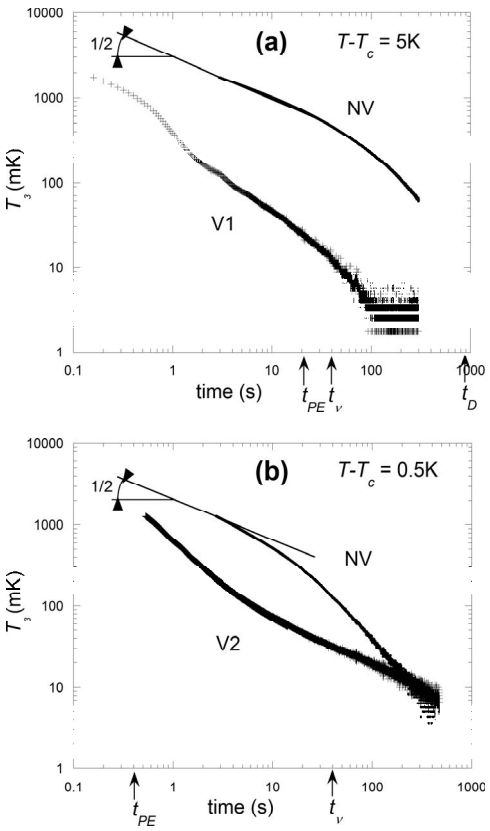

FIG. 7. Central thermistor (Th3) temperature relaxation ΔT_3 (log-log scales) after the heat pulse. Vibration, V1, V2; no vibrations, NV. (a) V1 at $T-T_c=5$ K and (b) V2 at $T-T_c=0.5$ K. The vertical arrows indicate the typical PE and viscous times. The horizontal arrow corresponds to the onset of the vibrational Rayleigh-Bénard instability (see text).

fact simply expresses that the heat exchange is affected by different processes, diffusion and PE alone for NV, and diffusion, PE and convection for V1 and V2.

In order to understand the different behaviors, one considers first the relative variations of the different time scales, t_D [Eq. (2)] and t_{PE} [Eq. (3)]. The longest and ultimate time scale is the diffusion time, t_D (5 K)=900 s and t_D (0.5 K) $\approx$4200 s (Table II). The shortest time is the PE time. From Table II, t_{PE} (5 K) $\approx$20 s and t_{PE} (0.5 K) $\approx$0.4 s.

Without vibration, equilibration indeed occurs by the PE and is faster at temperatures closer to T_c. In Fig. 7, the early times ($t \leqslant t_{\mathrm{PE}}$) correspond to relaxation slopes of 1/2, as expected [15,24].

When dealing with vibrations V1 and V2, another time is the viscous time [see Eq. (9)] corresponding to the viscous relaxation of the flow. From Table II, $t_\nu \approx 40$ s at all temperatures. Looking at Fig. 7, one indeed sees that the temperature relaxation is nearly completed for this time scale. Convection appears to relax temperature more efficiently than PE does. Indeed, the fluid is still in convective motion until the temperature gradients vanish. The temperature gradients at which convection stops can be estimated by calculating the temperature gradient for which Rv reaches its critical value ($\mathrm{Rv}_c \approx 2000$). The estimation, from Eqs. (12) and (13), gives $\Delta T=160$ mK for V1 at 5 K from T_c [Fig. 7(a)] and $\Delta T=210$ mK for V2 at 0.5 K from T_c [Fig. 7(b)]. This is precisely the time where the temperature relaxation slows down.

E. Bulk temperature evolution

1. Vibration V1

The local temperature evolutions at the Th1 and Th2 locations are described in Fig. 8. The maximum amplitude of the temperature increases are shown in Fig. 9. In the bulk, convection and PE compete. The former process heats up the fluid by convective flows. The second process heats up by the expansion of the HBL but cools by the contraction of a cold boundary layer (CBL) at the thermostat walls.

Far from the CP [T_c+5 K, Fig. 8(a)], the convective effect is prevailing. Between the start of the heat pulse at t_0 and the time t_1 where the convected HBL reaches Th1 or Th2, NV and V1 types behave the same. Bulk heating is only due to the PE. For times $t > t_1$, heating with vibration is more effective than without vibration, due to the HBL convection. After

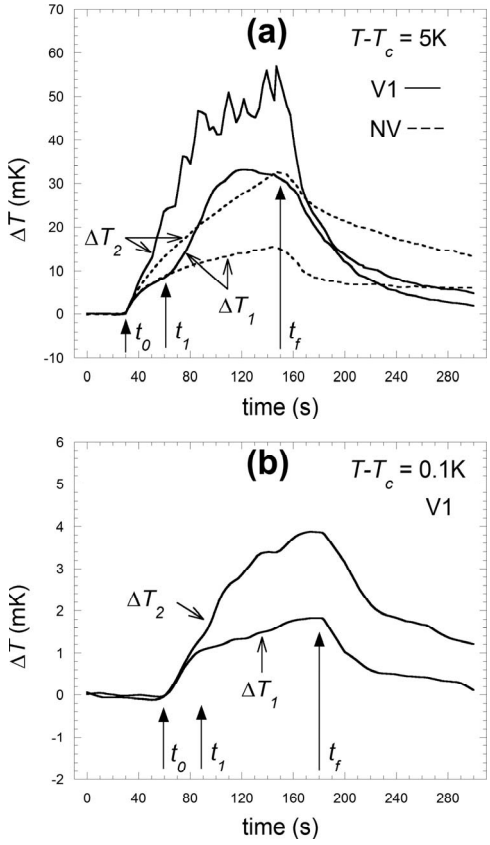

FIG. 8. Temperature evolution of the temperature in the bulk fluid (vibration V1, full line) and without vibration (NV, interrupted line) for temperature rise $\Delta T_1(t)=T_1(t)-T_1(\infty)$ at Th1 and $\Delta T_2(t)=T_2(t)-T_2(\infty)$ at Th2. t_0, beginning of the heat pulse; $t_{f'}$, end of the heat pulse; t_1, the HBL reaches Th1. (a) $T-T_c=5$ K, (b) $T-T_c=100$ mK. (All data have been filtered with an 8% numerical weighing procedure.)

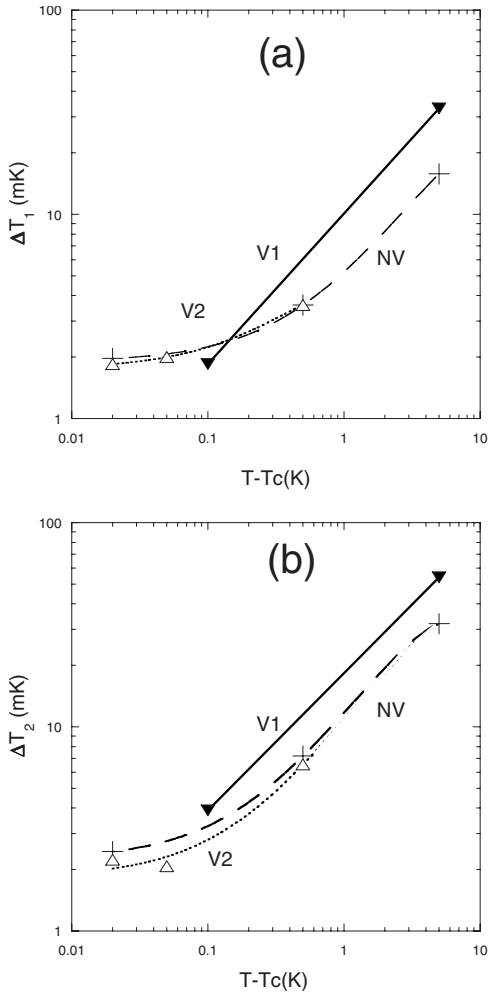

FIG. 9. Maximum temperature rise ΔT_{1M} (a) and ΔT_{2M} (b) with respect to temperature difference $T-T_c$ for vibrations V1 (full line, black triangles), V2 (dotted curve, open triangles) and no vibration NV (interrupted curve, crosses). (The curves are 2nd degree polynomial fits.)

the heat pulse has stopped ($t>t_f$, with $t_f=t_0+\delta t$), the relaxation to equilibrium with vibration is faster than without vibration, in agreement with the TH3 temperature relaxation as discussed in the preceding section. The acceleration of cooling is due to the thinning of the CBL by the former convection, as is observed under $1g$ acceleration [21]. A thinner layer, which pumps heat to the thermostat, indeed speeds up the bulk equilibration process. One also notes that convection makes the temperature T_1 and T_2 different. When convection is negligible with respect to PE (early times $t<t_1$ and $t\gg t_f$,) both T_1 and T_2 temperatures are the same.

Closer to the CP [$T_c+0.1$ K, Fig. 8(b)], the PE becomes much more efficient and the effect of convection is smaller. The temperatures T_1 and T_2 keep the same value a longer time at the beginning of the heat pulse Then, if one plots the maximum temperature increases ΔT_{1M} and ΔT_{2M} reached by T_1 and T_2 at the end of the heat pulse (Fig. 9), one sees that near T_c, the values observed for V1 can even become *lower* than those for NV. This is the hallmark of the increasing cooling efficiency by the CBL. The thermal layer is indeed thinned by the convection, making the thermal gradients—and the heat flux—higher. In addition, the temperature rise in the bulk is markedly lower than the one at 5 K (and similarly at 50 mK, when compared to the one at 100 mK). At first order analysis, this is due to the well-known divergence of C_V. Note that the divergence of C_p can also affect the process in a complex manner [15].

2. Vibration V2

The evolution of local temperatures, as measured by Th1 and Th2 thermistors, are presented in Fig. 10, for V2. The corresponding maximum amplitude of the temperature rise is shown in Fig. 9. In contrast to V1, the difference between vibration and no vibration remains small at all $T-T_c$. This is because, (i) the HBL reaches neither Th1 nor Th2, and (ii) the convection flow induced by the vibration remains confined around the HBL and does not thin the CBL. As a consequence, the cooling heat transfer at the cell wall is not enhanced. As for V1, the amplitude of the temperature rise also decreases with T approaching T_c, due to the increase of both C_p and C_V and the maximum temperature rise remains equal or slightly lower near T_c than for NV (Figs. 9 and 10).

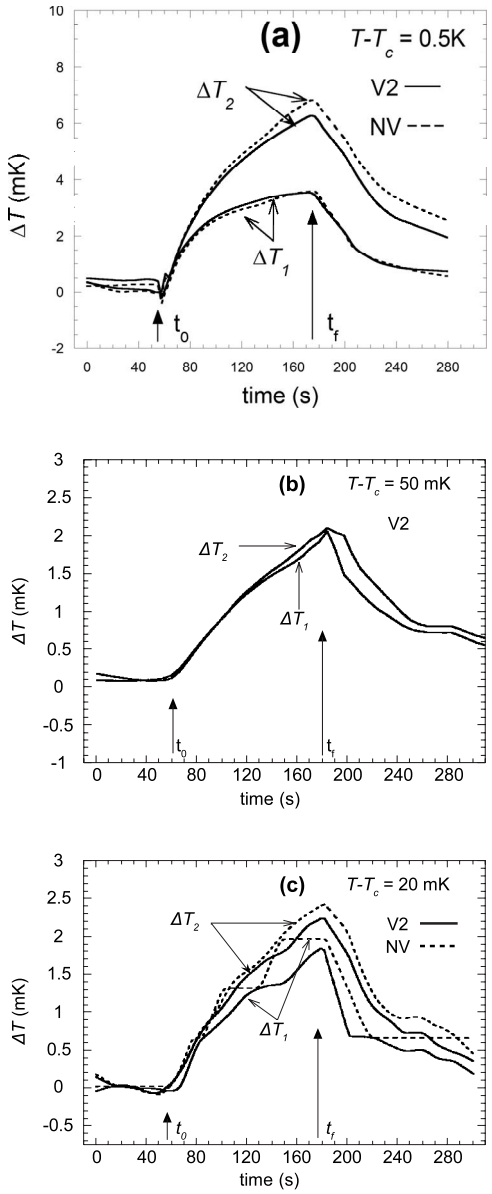

FIG. 10. Temperature evolution in the fluid (vibration V2, full line) and without vibration (NV, interrupted line) for temperature rise ΔT_1 at Th1 and ΔT_2 at Th2. t_0, beginning of the heat pulse; $t_{f'}$, end of the heat pulse. (a) $T-T_c=0.5$ K, (b) $T-T_c=50$ mK, and (c) $T-T_c=20$ mK (all data have been filtered with an 8% numerical weighing procedure).

IV. NUMERICAL SIMULATION

A. Vibration V1

An investigation of the regime V1 has been already reported by Jounet [25], in a 2D numerical simulation, using a van der Waals fluid model whose parameters were chosen as close as possible to those of CO_2. The evolution of density and fluid velocity was investigated. In spite of differences with the experimental geometry (square cell, point source, etc.), the simulation is in qualitative agreement with the present experiment. It reveals the same structures for approximately the same amplitudes and frequencies of vibration: double-plume along the vibration direction for large velocity amplitude and "pancake"-like structure elongated perpendicular to vibration.

B. Vibration V2

The case of a hot wire on the axis of an infinitely large and long cylinder filled with an incompressible and inviscid fluid, the whole submitted to high frequency vibrations, has been studied by Gershuni and Lyubomov [1]. In their 2D simulation of the present experimental situation, four convection rolls formed in the thermal density gradient of the HBL induce a convection pattern that spreads the HBL in pancake geometry similar to what is found in the present experiment. Jounet [25] has also described the main features of the density and velocity behavior, making reference to our preliminary data of the present experiment.

In the present work, we aim to determine what are the differences and similarities between highly compressible near-critical fluids and ideal gases, including a better account of the cell geometry, the finite size of the heating source, and experimental vibration amplitude (in the Jounet's work [25], the vibration amplitude is 10 times larger than the experimental one). We thus also performed 2D numerical simulations of the heat propagation process based on the Navier-Stokes equations with acoustics filtering procedure. A van der Waals equation of state was used, together with a mean-field behavior for the thermal conductivity. The model fluid is CO_2 at critical density and at temperature $T-T_c=1$ K, with values as close as possible to the experimental data. The heating power is 0.828 mW for 120 s sent from a circle of radius $r_0'=0.125$ mm. The cell radius, kept isothermal, is $R'=6$ mm. The length scales X, Y are then reduced by R'. The conductivities of boundaries are assumed infinite. The vibrations parameters are close to the experimental ones: frequency $f'=1.8$ Hz and amplitude $B'=0.38$ mm. The simulation is performed with the CFDACE computation code that resolves the velocity, pressure, and temperature fields described by the compressible Navier-Stokes equations using the finite volume method and the SIMPLER algorithm [26]. Grid computation is composed of 80 cells in the angular direction and 60 in the radial direction. A refinement of the grid is applied near the walls to correctly describe the boundary layers. The 2D cylindrical geometry is built with the structural grid mesh generator implemented in the CFDACE computation code. In order to reach times larger than the acoustic time scale, the acoustic filtering procedure is applied. This method is commonly used in the calculation involving low Mach number compressible flows [27]. The simulation results, which can only be qualitatively compared with the experimental data as the van der Waals equation is approximate and the present fluid is SF_6, are shown in Fig. 11 for the early times of the process. It is clearly seen that the HBL propagate perpendicularly to the vibration because of the existence of symmetrical counter-rotative convection rolls. These rolls were born in the strong density gradient at the boarder HBL—bulk, the latter showing a uniform density thanks to the PE.

In order to understand what is the role of the compressibility in the present phenomenon, we compare this van der

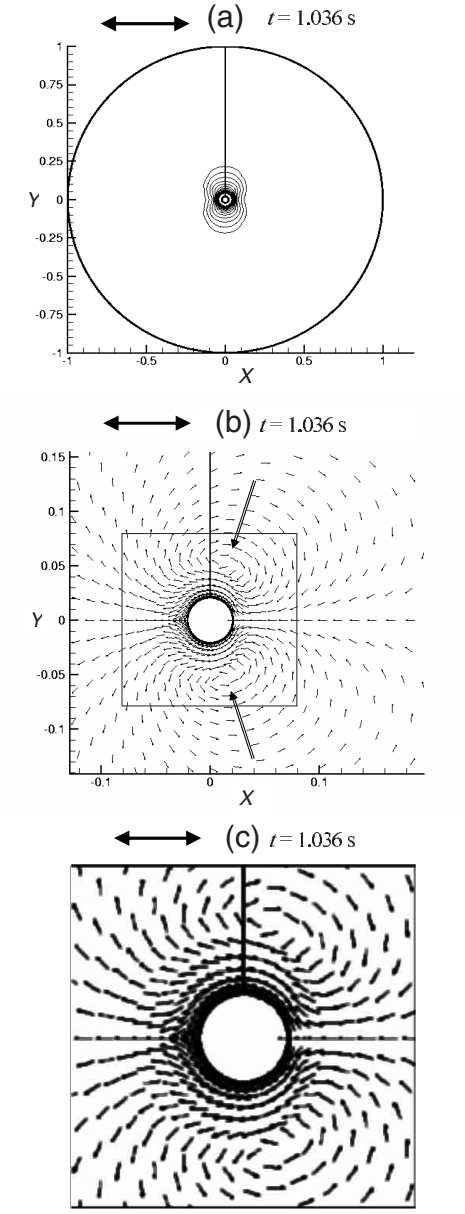

FIG. 11. Numerical simulation of the vibrational convection in a van der Waals fluid at $T-T_c=1$ K for a vibration with $f'=1.8$ Hz and $B'=0.38$ mm giving a pattern similar to the one in Fig. 4. The vibration direction is indicated by the double arrow. X and Y are the spatial coordinates in units of the cell radius R' (see text). (a) Temperature profile and (b) velocity field (small arrows) in arbitrary units near the onset of convection. (c) Enlarged view of the square in (b). Two rolls (indicated by two large open arrows) are clearly visible. Two symmetrical rolls will grow during the next period, forming in average four counter-rotative rolls.

Waals fluid and the corresponding ideal gas, obtained with the following conditions: $\rho=1.8$ kg m^{-3}, $T=T_c\approx 300$ K, ideal gas equation of state. Viscosity, thermal conductivity, heat capacities are constant and equal to the reference (background) values of the van der Waals gas [25]. The corresponding pattern is shown in Fig. 12. It is clear that the main difference between near-critical fluids and ideal gas lies in the spatial extension of the rolls. In the near-critical fluid, the low value of the thermal diffusivity makes the HBL confined

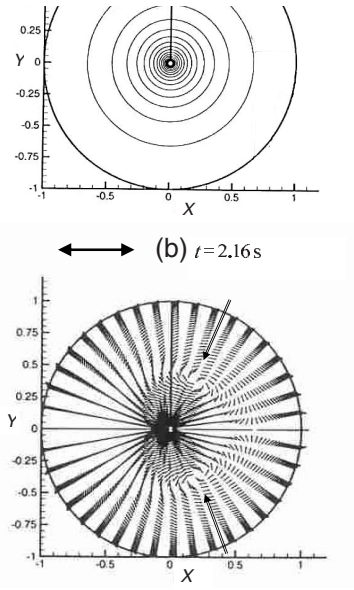

FIG. 12. 2D numerical simulation of the vibrational convection in an ideal gas at $T=300$ K$\approx T_c$ and the same vibration conditions as in Fig. 11. (a) Temperature profile. (b) Onset of two convection rolls (arrows). Two symmetrical rolls will grow at the next period, forming in average four counter-rotative rolls.

near the heat source. The rolls become thus smaller and smaller as one approaches the critical point.

The large compressibility of near-critical fluids therefore induces a fundamentally different behavior concerning the spatial extension of the initial convection zone. It is very likely that all the recent advances achieved in the Rayleigh-Bénard instability in near-critical fluids [21,27–31] concerning especially the Schwarzschild criterion and the heat transfer should also apply to the vibrational Rayleigh-Bénard instability.

V. CONCLUDING REMARKS

The effect of a linear harmonic vibration on near-critical fluid thermalization by a pointlike heat source is viewed as an initial displacement parallel to the vibration direction of two symmetrical hot plumes, the hot boundary layer, at a distance that is a function of vibration velocity only. Lateral spreading of the two extremities of the plumes proceeds further as hot "pancakes." When the amplitude of the vibration is small enough, only one hot boundary layer pancake, centered on the source, is present. Thermalization is ensured by the competition between convective flows, the "piston-effect" adiabatic heating by the hot boundary layer and the similar cooling effect at the cell walls.

The initial displacement of the hot fluid can be understood as an effect of vibration acceleration, similar to the onset of a classical Rayleigh-Bénard instability, while the further displacement perpendicular to the vibration direction can be viewed as a vibrational Rayleigh-Bénard instability. The latter instability can be observed in an ideal fluid, as shown by a simulation. The large compressibility and the critical

slowing down of the thermal diffusion in near-critical fluids induce a number of fundamental changes that deserves further investigation. In particular, convection starts by rolls confined in the hot boundary region, which becomes thinner and whose density profile becomes steeper as the critical point is neared.

These paradoxical behaviors where heat is convected either parallel or perpendicular to the vibration direction depending on the control parameters show that the phenomenology of thermal vibrational phenomena under reduced gravity is worthy of further investigation. The frequent use of supercritical fluids in space motivates such studies to enhance our knowledge of fluid behavior and fluid management in space conditions.

ACKNOWLEDGMENTS

This work has been partially supported by the French spatial agency CNES and Russian Foundation for Basic Research, Contracts Nos. 05-02-17106, and 06.01-00281. The authors of the paper gratefully thank V. S. Nikolayev for his careful reading and kind comments. The authors express their gratitude to V. P. Nikitski, ISTC General Director for support of this work and French and Russian cosmonauts S. Avdeev, V. Afanasiev, J.-P. Haignere, and G. Padalka for performing the space experiments on the orbital Mir station. The authors are grateful to A. Ivanov, V. Levtov, and V. Romanov for using the shaker and help in carrying out the experiments. The authors also thank A. Zyuzgin for help in a program development for the Alice-2 instrument.

[1] G. Z. Gershuni and D. V. Lyubimov, *Thermal Vibrational Convection* (Wiley, New York, 1998).
[2] See, e.g., A. Onuki, *Phase Transition Dynamics* (Cambridge University Press, Cambridge, 2002), and references therein.
[3] V. Polezhaev, V. Emelianov, A. Ivanov, A. Kalmykov, D. Beysens, and Y. Garrabos, Cosmic Res. **39**, 187 (2001) [translated from Kosm. Issled. **39**, 201 (2001)].
[4] R. Marcout, J.-F. Zwilling, J.-M. Laherrere, Y. Garrabos, and D. Beysens, Microgavity Q **5**, 162 (1995).
[5] Y. Garrabos, B. Le Neindre, R. Wunenburger, C. Lecoutre-Chabot, and D. Beysens, Int. J. Thermophys. **23**, 997 (2002), and references therein.
[6] B. Zappoli, D. Bailly, Y. Garrabos, B. Le Neindre, P. Guenoun, and D. Beysens, Phys. Rev. A **41**, 2264 (1990).
[7] A. Onuki, H. Hao, and R. A. Ferrell, Phys. Rev. A **41**, 2256 (1990); A. Onuki, and R. A Ferrell, Physica A **164**, 245 (1990).
[8] M. Bonetti, F. Perrot, D. Beysens, and Y. Garrabos, Phys. Rev. E **49**, R4779 (1994).
[9] P. Guenoun, D. Beysens, Y. Garrabos, F. Kammoun, B. Le Neindre, and B. Zappoli, Phys. Rev. E **47**, 1531 (1993).
[10] H. Klein, G. Schmitz, and D. Woermann, Phys. Rev. A **43**, 4562 (1991).
[11] R. P. Behringer, A. Onuki, and H. Meyer, J. Low Temp. Phys. **81**, 71 (1990).
[12] H. Boukari, J. N. Shaumeyer, M. E. Briggs, and R. W. Gammon, Phys. Rev. Lett. **65**, 2654 (1990).
[13] R. A. Wilkinson, G. A. Zimmerli, H. Hao, M. R. Moldover, R. F. Berg, W. L. Jonson, R. A. Ferrell, and R. W. Gammon, Phys. Rev. E **57**, 436 (1998).
[14] R. De Bruijn, R. J. J. Van Diest, T. D. Karapantsios, A. C. Michels, W. A. Wakeham, and J. P. M. Trusler, Physica A **242**, 119 (1997).
[15] Y. Garrabos, M. Bonetti, D. Beysens, F. Perrot, T. Frohlich, P. Carles, and B. Zappoli, Phys. Rev. E **57**, 5665 (1998).
[16] P. Carlès and K. Dadzie, Phys. Rev. E **71**, 066310 (2005).
[17] K. Kawasaki, Phys. Rev. A **1**, 1750 (1970).
[18] B. Quentrec, J. Phys. (Paris) **40**, L-257 (1979).
[19] A. Onuki, Phys. Rev. E **55**, 403 (1997).
[20] K. A. Gillis, I. I. Shinder, and M. R. Moldover, Phys. Rev. E **72**, 051201 (2005).
[21] B. Zappoli, A. Jounet, S. Amiroudine, and A. Motjabi, J. Fluid Mech. **388**, 389 (1999).
[22] See, e.g., V. I. Polezhaev and E. B. Soboleva, Fluid Dyn. **40**, 209 (2005), and references therein; V. I. Poleshaev and E. B. Soboleva, Izv. Akad. Nauk, Mekh. Zhidk. Gaza **14**, 48 (2005).
[23] T. Frohlich, S. Bouquet, M. Bonetti, Y. Garrabos, and D. Beysens, Physica A **218**, 419 (1995).
[24] R. A. Ferrell and H. Hao, Physica A **197**, 23 (1993).
[25] A. Jounet, Phys. Rev. E **65**, 037301 (2002).
[26] S. V. Patankar, *Numerical Heat Transfer and Fluid Flow* (Hemisphere, New York, 1980).
[27] V. Nikolayev, A. Dejoan, Y. Garrabos, and D. Beysens, Phys. Rev. E **67**, 061202 (2003).
[28] S. Amiroudine and B. Zappoli, Phys. Rev. Lett. **90**, 105303 (2003).
[29] A. B. Kogan, D. Murphy, and H. Meyer, Phys. Rev. Lett. **82**, 4635 (1999).
[30] A. Furukawa, H. Meyer, and A. Onuki, Phys. Rev. E **71**, 067301 (2005).
[31] Y. Chiwata and A. Akira Onuki, Phys. Rev. Lett. **87**, 144301 (2001).